From anisotropic dots to smooth RFe$_2$(110) single crystal layers (R = rare earth)

A. Mougin[a], C. Dufour, N. Maloufi, K. Dumesnil, and Ph. Mangin

Laboratoire de Physique des Matériaux[b], Université Henri Poincaré - Nancy I, BP 239, 54506 Vandœuvre-lès-Nancy, France

Abstract. Single crystal RFe$_2$(110) films were grown by molecular beam epitaxy to a total thickness of 1000 Å at different substrate temperatures ranging from 450 °C to 660 °C. The first stages of growth and the surface morphology of the deposited layers have been studied using Reflection High Energy Electron Diffraction (RHEED) and Atomic Force Microscopy (AFM). The growth is first strained but further deposit induces the formation of three-dimensional fully relaxed islands. Subsequently, the morphology of the RFe$_2$(110) nanosystems evolves from anisotropic dots to a smooth surface, as a function of the preparation parameters, *i.e.* nominal thickness and substrate temperature. It also depends on the rare earth involved in the compound.

PACS. 61.14.Hg Low-energy electron diffraction (LEED) and reflection high-energy electron diffraction (RHEED) – 61.16.Ch Scanning probe microscopy: scanning tunneling, atomic force, scanning optical, magnetic force, etc. – 71.20.Lp Intermetallic compounds

1 Introduction

Three-dimensional nanostructured magnetic materials are currently investigated for their fundamental and technological properties, since their basic magnetic properties can be drastically different from those of a continuous film. To elaborate such three-dimensional magnetic nanostructures, the self-organized growth is an interesting alternative to lithography techniques.

Up to now, such a preparation process has been mainly used for electronic and optoelectronic materials [1–5]. It has been shown that a strain relaxation can be achieved by the formation of nanoscopic islands; the interaction between the islands through the local strain of the substrate is at the origin of their regular arrangement [3–5]. Simultaneously, theoretical analysis of the growth of heteroepitaxial islands has been developed. In particular, the relevant parameters were found to be on one hand, the lattice mismatch between the deposited material and the substrate, and, on another hand, the nominal coverage [6].

In the case of transition metals, using metallic or oxide substrates, a wide variety of surface morphology has been observed [7–10]. Due to advances in experimental techniques, a significant control over the growth of epitaxial metallic films is now possible and, under certain conditions, one can tailor the structural properties of the layers.

Bulk RFe$_2$(110) Laves Phases compounds (R is a rare earth) gather together the strong magnetocrystalline anisotropy of rare earth and the important exchange interaction of iron. Consequently, they exhibit exceptionally large magnetostriction at room temperature [11]. Thus, single crystal strained systems of RFe$_2$ compounds with reduced lateral dimensions are of great interest, because of their underlying physics and potential application as sensor or actuator devices. Recently, the growth of RFe$_2$ compounds has been achieved by different techniques: sputtering, laser ablation or molecular beam epitaxy [12–14]. Depending on the substrate, on its orientation and on the deposition conditions, [111] or [110] growth directions have been obtained. These RFe$_2$ nanostructures exhibit exciting new magnetic properties. We showed that RFe$_2$(110) layers are strained compared to bulk compounds and both sign and values of strains are explained with a model of differential thermal contraction between the film and the substrate [15]. Mössbauer spectrometry and magnetization measurements demonstrated that the magnetic anisotropy is modified in magnetostrictive RFe$_2$(110) layers compared to corresponding bulk systems [16]. These experimental observations have been reproduced by a model, which includes the various energy terms governing the magnetization direction. In fact, the enhancement of the magnetoelastic term, due to the strains, accounts well for the observed modifications of easy magnetization directions in RFe$_2$(110) layers [16]. It has also been demonstrated that the macroscopic magnetization reversal strongly depends on the morphology of DyFe$_2$(110) deposits: continuous layers or isolated dots do not exhibit the same macroscopic behavior [17]. Nevertheless, to our knowledge, very few other results concerning the morphology of the layers have been published [18].

[a] e-mail: mougin@lps.u-psud.fr
[b] UMR 7556 CNRS

In this paper, the epitaxial growth of $RFe_2(110)$ compounds is reported in details, from Reflection High Energy Electron Diffraction (RHEED) and Atomic Force Microscopy (AFM) measurements. The first stage of the $ErFe_2$ growth along [110] is described (Sect. 3). The morphology evolution of $DyFe_2(110)$ layers is then presented in Section 4 as a function of the preparation parameters (nominal thickness and substrate temperature) and compared to the morphology of $ErFe_2(110)$ systems (Sect. 5).

2 $RFe_2(110)$ preparation and experimental set-up

The samples were prepared by molecular beam epitaxy in an ultrahigh vacuum chamber whose base pressure was typically 4×10^{-11} torr. Following the procedure described by Kwo *et al.* [19], the $Al_2O_3(11\bar{2}0)$ substrate is covered at 850 °C by a 500 Å $Nb(110)$ buffer layer [14]. Because of the large lattice mismatch between bulk niobium and bulk Laves phases compounds under consideration (which varies from 9.92% to 12.58% depending on the rare earth involved in the compound [15]), the direct growth of $RFe_2(110)$ compounds on the $Nb(110)$ layer was not possible. This niobium layer has been covered with a thin iron template layer (15 Å at 550 °C) [14]. Intermixing between iron and niobium leads to a surface alloy referred as $NbFe\varphi$ exhibiting a rectangular mesh, whose main directions (called $a_{NbFe\varphi}$ and $b_{NbFe\varphi}$) are parallel to those of niobium. This $NbFe\varphi$ buffer is suitable for the $RFe_2(110)$ single crystal growth ($a_{NbFe\varphi} = 7$ Å and $b_{NbFe\varphi} = 4.8$ Å). The lattice mismatches between RFe_2 and $NbFe\varphi$ are then anisotropic and reduced, especially along the [001] direction (where it varies from 4.17% to 10.02% depending on R) [15]. The epitaxial relationships between the layers are:

$$[001]Nb//a_{NbFe\varphi}//[001]RFe_2 \quad \text{and}$$

$$[\bar{1}10]Nb//b_{NbFe\varphi}//[\bar{1}10]RFe_2.$$

The RFe_2 growth has been achieved by codeposition of iron and rare earth on the $NbFe\varphi$ buffer. The deposition rates are controlled *in situ* by quartz balances and optical sensors; the total deposition rate is 5 Å per minute. The chemical composition of the compounds has been checked *a posteriori* by microprobe analysis and was found to be ± 2% of the RFe_2 stoichiometric composition.

Reflection High Energy Electron Diffraction with an incident angle of about 1° and a beam energy of 30 keV permitted the *in situ* study of the growth mode and of the crystal quality of the surface [14]. The as-deposited samples were then taken out of the chamber and immediately observed using a Park Scientific Instrument atomic force microscope (AFM). The experimental set-up was an Autoprobe CP of Park Scientific instrument working in contact mode at constant force. The probes used were of two kinds: microlevers of siliconnitrid with sharpened tip and a radius of curvature of 200 Å for relatively flat surfaces, and ultralevers of silicon with a conical tip presenting a radius of curvature of 100 Å for rough layers. After a careful correction of the image slope (which depends on the scanning conditions), we
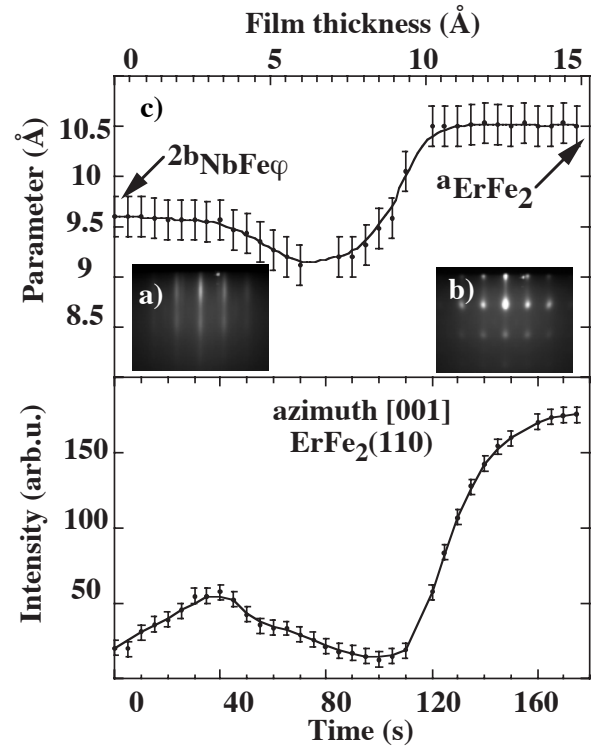

Fig. 1. $ErFe_2(110)$ grown at 550 °C: (a) [001] azimuth RHEED pattern for a deposited thickness of 3 Å, (b) [001] azimuth RHEED pattern for a deposited thickness of 12 Å, (c) surface lattice parameter and diffracted intensity as a function of the deposited thickness.

used a version of the public domain analysis software NIH (Image SXM) that has been extended to handle the loading, display and analysis of scanning microscope images. This allowed the real determination of the surface morphology and more precisely the dot size and distribution; as an example, the roughness (standard deviation from the average z value) was systematically extracted from $2 \ \mu m \times 2 \ \mu m^2$ images whereas line scans across images allowed the measurement of the island dimensions. Moreover, Scanning Electron Microscopy experiments (not presented here) were performed to exclude misleading information produced by contaminated AFM tips.

3 First stages of growth: 0–15 Å of $ErFe_2(110)$

Let's first note that the RHEED patterns observed from the $NbFe\varphi$ buffer exhibit streaks indicative of a smooth surface and, from AFM measurements, its surface roughness is about 3 Å. The RHEED patterns along the [001] azimuth obtained after a 3 Å and a 12 Å deposition of $ErFe_2(110)$ at 550 °C are presented in Figures 1a and 1b. Whereas the 3 Å layer exhibits continuous diffraction lines, at the same position as the $NbFe\varphi$ buffer ones, these have turned into spots when the deposited thickness reaches 12 Å.

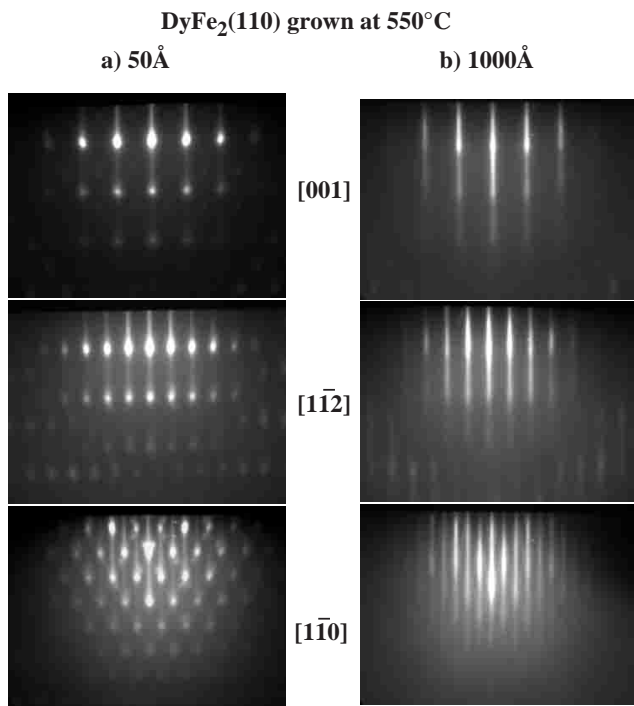Figure 1c shows the evolution of the surface lattice parameter and of the diffracted intensity as a function

DyFe$_2$(110) grown at 550°C

a) 50Å   **b) 1000Å**

[001]

[1$\bar{1}$2]

[1$\bar{1}$0]

Fig. 2. RHEED patterns along the [001], [1$\bar{1}$2] and [1$\bar{1}$0] azimuths of DyFe$_2$(110) layers grown at 550 °C for two thicknesses: 50 Å (a) and 1000 Å (b).

Fig. 3. Details of RHEED patterns along the [001] and [1$\bar{1}$0] azimuths of 50 Å DyFe$_2$(110) grown at 550 °C.

lands. These islands contribute to the build-up of elastic strains and their growth, coalescence and renucleation is energetically too expensive. Thus, in a next stage, three-dimensional islands form; they are lattice-matched at their base but are largely strain-relieved near their top and side walls. Moreover, the formation of dislocations could also contribute to the relaxation of strains in the islands. Preliminary Transmission Electron Microscopy results show that, in RFe$_2$(110) samples, the complete relaxation coincides with the formation of edge dislocations in the {111} planes. The formation of three-dimensional relaxed islands with the increase of the deposited thickness is also consistent with the *ex situ* measured strains. In fact, in a previous paper [15], we have demonstrated that RFe$_2$(110) layers are submitted to an ϵ_{xy} negative shear. This shear is a purely thermal shear and can be explained by the different thermal expansion coefficients in the substrate and in the compounds: it occurs when the sample is cooled from the growth temperature, where it is fully relaxed, to room temperature.

4 Influence of the preparation parameters on DyFe$_2$(110) samples morphology

4.1 Nominal thickness

Different DyFe$_2$(110) layers, with thicknesses ranging from 50 Å to 1000 Å, have been grown at a given substrate temperature (T_S = 550 °C) in order to investigate the influence of the deposited thickness on the sample morphology.

Figure 2 shows RHEED patterns obtained for the films with 50 Å ((a)-left side) and 1000 Å ((b)-right side) nominal thickness. Three main azimuths are reported: [001], [1$\bar{1}$2] and [1$\bar{1}$0]. For the 50 Å layer, the diffraction patterns are still spotty and similar to the ones observed after a 12 Å deposition (Fig. 1b) which implies that the surface is rough and constituted of three-dimensional structures. For the 1000 Å layer, the patterns exhibit well defined and intense streaks which are characteristic of a flat surface. The change from spot diffraction to streak diffraction when the deposited thickness increases from 50 Å to 1000 Å indicates that the islands coalesce in this thickness range. One has to note that, whatever the deposited thickness is, the samples are unique single crystals, without twins as confirmed by grazing incidence X-ray diffraction [15].

Further, chevron patterns have been observed along the [1$\bar{1}$0] and [001] azimuths (Fig. 3) but never along the other directions. Such RHEED patterns with chevrons are the superposition of diffracted patterns from nearly
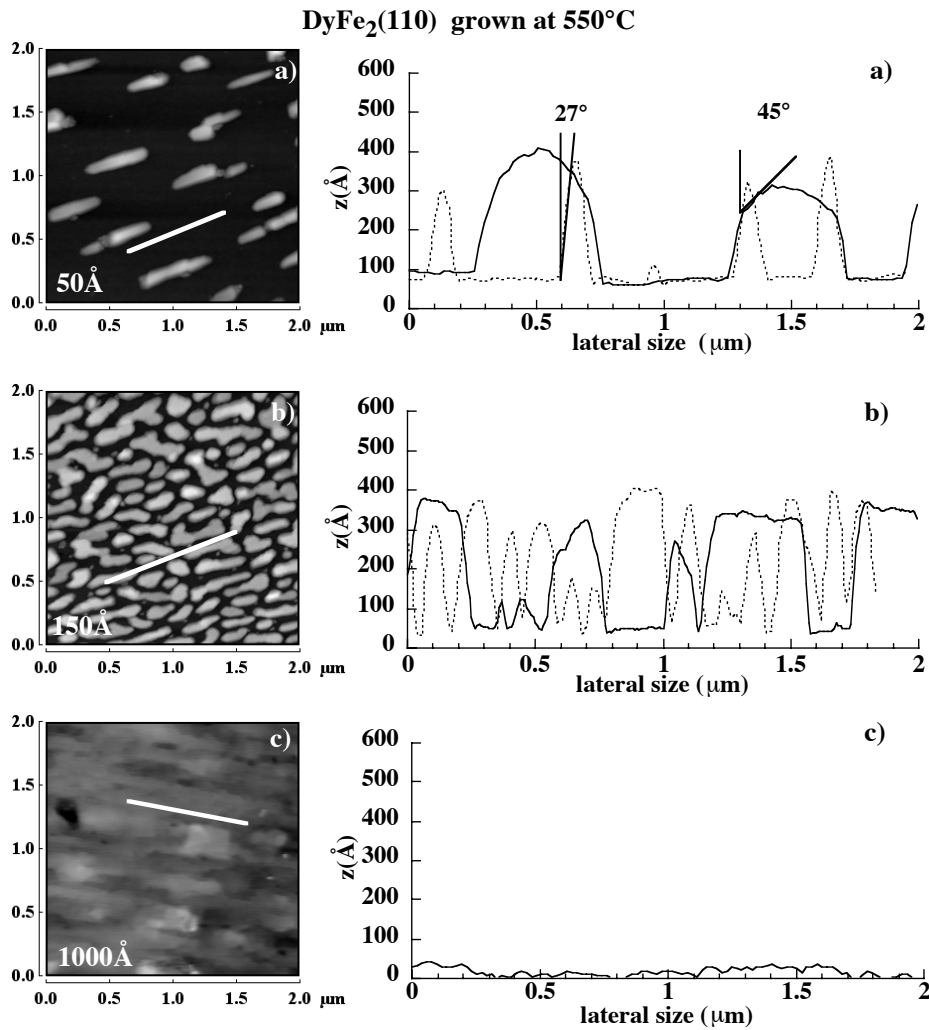
of the deposited film thickness for the same sample in the 0–15 Å range. The experimental values are deduced from the analysis of a set of [001] azimuth RHEED patterns; the parameter is calibrated to the buffer one.

For deposited thicknesses smaller than 4 Å, the RFe$_2$ in-plane parameter is close to the buffer layer one, whereas the diffracted intensity increases very slowly. Both evolutions account for a two-dimensional matched growth. Despite experimental observations, we cannot distinguish between the growth of large matched islands or the growth of completed matched layer on the substrate. When the nominal deposited thickness increases, an intense diffuse background appears. Simultaneously, the in-plane parameter decreases smoothly, which is still under investigation. After 9 Å, RHEED patterns exhibit more and more intense diffraction spots. In the same thickness range, the in-plane parameter increases abruptly and, after a 10 Å deposit, it reaches the RFe$_2$ bulk parameter at the deposition temperature. The pattern does not evolve so much and remains spotty (Fig. 1b), which indicates that three-dimensional fully relaxed ErFe$_2$(110) islands have been grown. A qualitative similar behaviour has been observed during the growth process of others RFe$_2$(110) compounds in the same conditions.

The occurrence of three-dimensional RFe$_2$(110) relaxed islands after a short phase of two-dimensional matched growth is close to the Stranski-Krastanov growth mode [20]. Such a growth is often observed when there is a large misfit between the buffer and the film. It is characterized by the formation of a thin lattice-matched wetting layer is followed by the nucleation of two-dimensional is-

Fig. 4. 2 μm $\times$ 2 μm^2 AFM images (left side) for 50 Å (a), 150 Å (b) and 1000 Å (c) DyFe$_2$(110) layers grown at 550 °C. Corresponding height profiles (right side) along the [1$\bar{1}$0] direction (bold line) reported on the images and along the perpendicular [001] direction (dotted line).

two-dimensional surface structures and from inclined ones. These patterns are thus characteristic of dots with a "truncated pyramid" shape [21,22]. From the angles between the chevron lines and the [110] growth direction (53$\pm$1° along the [1$\bar{1}$0] azimuth and 90$\pm$1° along [001]), one can determine that the facets surrounding the dots are parallel to {332} and {010} planes.

Figure 4 shows the AFM images (left side) for 50 Å, 150 Å and 1000 Å DyFe$_2$(110) layers grown at 550 °C and the corresponding height profiles (right side) along the [001] (dotted curve) and [1$\bar{1}$0] (plain curve) directions. The [1$\bar{1}$0] direction is indicated in the pictures by a bold white line.

The 50 Å nanosystem (Fig. 4a) is constituted of isolated anisotropic dots. The dots are 260 Å high; they are elongated along the [1$\bar{1}$0] direction, where their length is about 4000 Å; they are four times smaller in the perpendicular [001] direction. The dots present slightly elliptic shapes. The profile is clearly pyramid along the [001] direction and presents a more rounded shape along the per-

pendicular direction. However, along this latter [1$\bar{1}$0] direction, facets can be observed on the top of the dots. The facet measured angles are consistent with the values deduced from RHEED patterns analysis. As reported by many other groups, one has to keep in mind that a smoothing effect, attributed to the well known tip-image convolution, may occur [21,22].

When the nominal thickness increases (150 Å, Fig. 4b), the coverage of the substrate increases considerably. The number of structures is larger, whereas their dimensions do not change so obviously. For this larger coverage, the "truncated pyramids" are no more obvious. Nevertheless, the islands keep a favored orientation and start to coalesce. As the growth and coalescence continue, the coverage increases while their density decreases.

For nominal thickness of 1000 Å, Figure 4c, the DyFe$_2$(110) film is continuous and flat, in agreement with the RHEED patterns of Figure 2. The height profile provides in this case no information about the layer height but about the surface roughness which is around 20 Å.
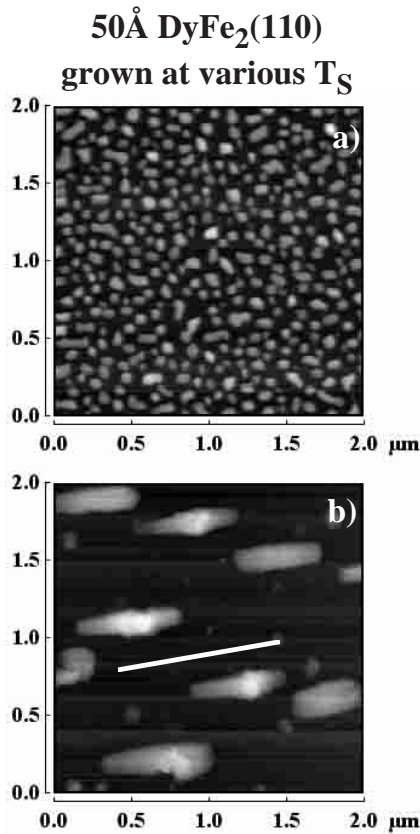
50Å DyFe$_2$(110)
grown at various T$_S$

Fig. 5. 2 μm $\times$ 2 μm^2 AFM images for 50 Å DyFe$_2$(110) layers grown at (a) 460 °C and (b) 660 °C. The [1$\bar{1}$0] direction (bold line) is reported on the (b) image.

50Å DyFe$_2$(110)
grown at various T$_S$

Fig. 6. Size distributions of 50 Å DyFe$_2$(110) layers grown at T_S = 460 °C (a), 550 °C (b) and 660 °C (c).

In summary, from both RHEED and AFM results, at T_S = 550 °C, the morphology of the DyFe$_2$(110) layers strongly depends on the nominal deposited thickness and evolves from anisotropic and isolated dots to a continuous film with low surface roughness.

4.2 Substrate temperature

In order to investigate the influence of the substrate temperature during the deposition process on the morphology, DyFe$_2$(110) layers with a given thickness (50 Å) have been prepared at different temperatures. The temperature study is restricted to the 460–660 °C range. In fact, for deposition temperature lower than 450 °C, the deposited layers are polycrystal or amorphous, whereas for preparation temperatures higher than 660 °C, the samples become textured polycrystal layers.

The Figure 5 shows the AFM images of 50 Å DyFe$_2$(110) nanosystems grown at T_S = 460 °C (a) and 660 °C (b). The 50 Å DyFe$_2$(110) morphology grown at intermediate temperature (550 °C) has already been presented (Fig. 4a). One can note that all 50 Å layers are discontinuous and constituted of isolated dots, whatever
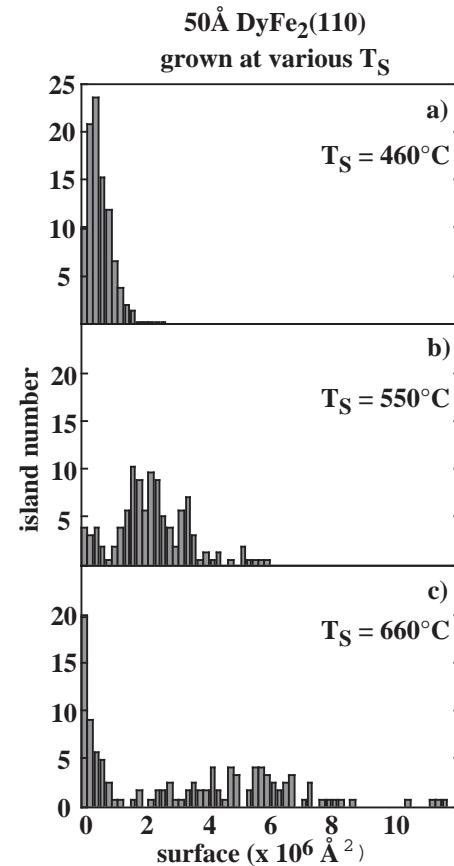
the growth temperature is. For these small thicknesses, the large areas between the islands are almost flat. The number of dots per surface unit increases as the temperature is lowered, whereas the dot size is reduced. In the low temperature case, where the island density is high, the dots seem to have a rounded shape and they become more and more anisotropic when the temperature is higher. The corresponding size distributions are reported in Figure 6. The 460 °C grown layer (Fig. 6a) presents a narrow size distribution centered around 1000 $\times$ 1000 Å^2. When the deposition temperature increases, the size distribution still exhibits a peak centered around this surface value, but the main peak is broader and shifts towards larger surfaces (4250 $\times$ 800 Å^2 for T_S = 550 °C and 4800 $\times$ 1000 Å^2 for T_S = 660 °C). Nucleation of islands leads to a distribution of smaller islands [21] and high temperature favors surface mobility of the ad-atoms, thus coarsening and ripening, and finally the increase of the average dimensions of the dominant structures.

The drastic influence of the preparation temperature is also obvious if one compares two 1000 Å DyFe$_2$(110) samples grown respectively at 550 °C and 660 °C. The former presents a low surface roughness (Fig. 4c) whereas the latter, grown at higher temperature (660 °C) still exhibits large islands elongated in the [1$\bar{1}$0] direction, as shown
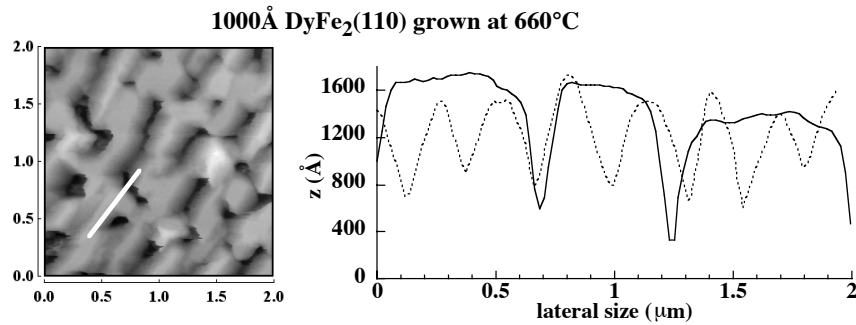
Fig. 7. 2 μm $\times$ 2 μm^2 AFM image (left side) for a 1000 Å DyFe$_2$(110) layer grown at 660 °C. Corresponding height profiles (right side) along the [1$\bar{1}$0] direction (bold line) reported on the images and along the perpendicular [001] direction (dotted line).

in Figure 7. Despite the relatively large thickness, the film is not fully coalesced and the islands have sharp pyramid shape.

Thus, the dot shape, size and density as well as the coalescence process depend strongly on the substrate temperature for T_S varying between 450 °C and 660 °C.

4.3 Summary and discussion

Figure 8 summarizes the evolution of the coverage, the density and the average height of the islands for a set of DyFe$_2$(110) layers as a function of the nominal thickness, ranging from 50 Å to 1000 Å, and for the various growth temperatures (460 °C, 550 °C and 660 °C).

For any thickness, the higher preparation temperature, the lower coverage and density of dots, but the higher the dots. The evolution *versus* thickness is different and the growth process can thus be analyzed in two stages:

i) First, for thicknesses smaller than 150 Å, the density increases quickly, whereas the average dimensions of the dots do not change so much (at least for the two lower temperatures). This process insures the coverage evolution.

ii) As the deposited thickness reaches about 200 Å, the island density decreases and the dimensions of the islands increase. At this stage, nucleation does not contribute anymore to the growth and surface diffusion becomes predominant [23]. As deposition goes on, coalescence gives rise to continuous and fully covered surfaces for 460 °C and 550 °C substrate temperatures and the deposited thickness required to obtain a continuous layer decreases with the substrate temperature. If the preparation temperature is higher (660 °C), atoms diffusing more easily on the surface join the existing islands [21,23]. Therefore, the island density decreases and the structures grow but the fully coalescence is delayed: even for deposited thickness as large as 1000 Å, the surface coverage remains limited (85%) and the layer is still constituted of disconnected large islands, as shown previously in Figure 7.

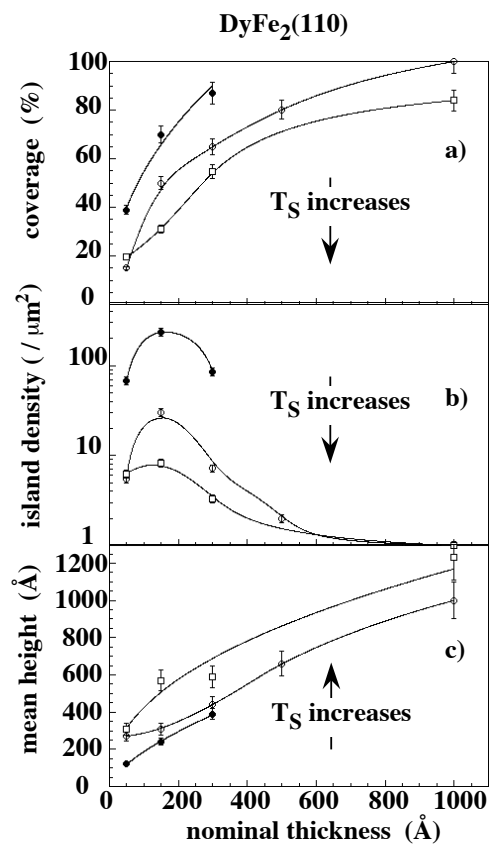Figure 9 shows the evolution of the anisotropy factor of the grown structures *versus* the nominal thickness. This

Fig. 8. Evolution of (a) the coverage, (b) the density, (c) the average height of the islands as a function of the DyFe$_2$ nominal thickness, with T_S = 460 °C (filled circles), 550 °C (open circles) and 660 °C (open squares). The lines are guides to the eyes.

factor is defined as the ratio between the dimensions along the [1$\bar{1}$0] and [001] directions. The length to width ratio is ranging from 5 to 2 for small thicknesses (characterized by isolated structures). When the structures coalesce, for increasing deposited thickness, the anisotropic factor is reduced to 1. For the 660 °C deposited layers (squares), the length to width ratio never reaches this value because the sample remains discontinuous and formed of anisotropic islands.
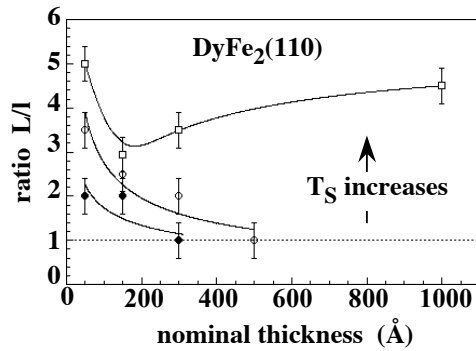
Fig. 9. Evolution of the anisotropy factor (ratio between the dimensions along the [1$\bar{1}$0] and [001] directions) as a function of the DyFe$_2$ nominal thickness, with $T_S = 460$ °C (filled circles), 550 °C (open circles) and 660 °C (open squares). The lines are guides to the eyes.

According to Tersoff *et al.* calculations [24], when a square based island reaches a critical size, elongation is favoured to maintain a "low mismatch strain", at least along one of the island axes. The stress being then anisotropic, the island should align itself perpendicular to the direction of maximum strain (*i.e.* direction presenting the larger mismatch with the buffer). However, to account for the elastic energy reduction which occurs in the isolated islands, some authors [25] introduce an effective mismatch, noted m_{eff}. This effective mismatch strongly depends on the aspect ratio (L/H), on the angle γ which defines the facets of the island and on the usual mismatch m. In our case, the DyFe$_2$(110) islands being aligned along the [1$\bar{1}$0] direction, the effective mismatch, contrarily to the nominal mismatch, is expected to be larger along [001] than along [1$\bar{1}$0] [15,24,25].

5 Influence of the compound on the morphology: ErFe$_2$(110) and DyFe$_2$(110)

In order to further investigate the growth mechanism, ErFe$_2$(110) samples have been compared to DyFe$_2$(110) ones. Figure 10 shows the AFM images of 50 Å (a) and 150 Å (b) ErFe$_2$(110) layers grown at $T_S = 550$ °C and should thus be compared to those of Figures 4a and b. Both ErFe$_2$(110) layers are discontinuous, constituted of small isolated dots. The coverage increases from 36% for the 50 Å sample to 50% for the 150 Å one. The difference with the DyFe$_2$ system is obvious, especially for the 50 Å layers: the density of dots is much larger (88/μm^2 for ErFe$_2$ compared to 10/μm^2 for DyFe$_2$) and their dimensions are 4 to 5 times smaller (1000 × 800 Å^2). Moreover, the anisotropy ratio is much smaller, since it is close to 1.25 compared to 4 for DyFe$_2$. In the case of 150 Å thick layers, the ErFe$_2$ structures are again smaller than the DyFe$_2$ ones (about 30%) and the anisotropic shape has almost disappeared, since the islands are approximately 3000 Å diameter dots.
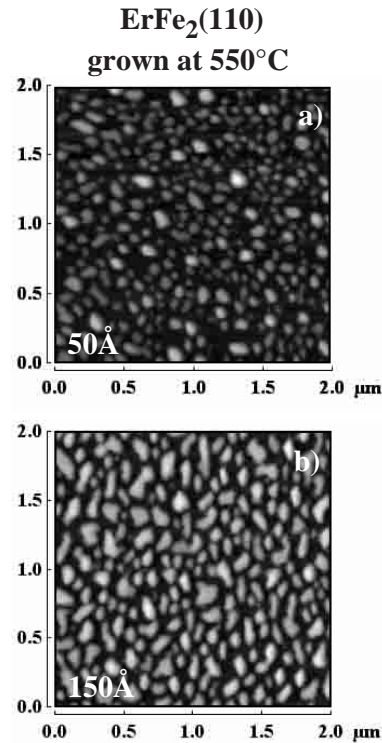
ErFe$_2$(110) grown at 550°C

Fig. 10. 2 μm × 2 μm^2 AFM images for 50 Å (a) and 150 Å (b) ErFe$_2$(110) layers grown at 550 °C.

Thus, despite the large similarities in structural and chemical properties between different RFe$_2$ compounds, the morphology of the RFe$_2$(110) layers depends on the Laves phase system.

The significant difference between the DyFe$_2$ and ErFe$_2$ deposition is the nominal mismatch with the buffer layer, which depends on the rare earth involved in the compound, and is reduced from 0.7% in ErFe$_2$ compared to DyFe$_2$ [15].

If one considers that the lattice mismatch is the dominant factor determining dot dimensions, one would expect an increase in mismatch to result in a decrease of the dots dimensions; such a behaviour has been observed in In$_x$Ga$_{1-x}$As/GaAs [26]. Our experimental results are obviously not consistent with this simple hypothesis. One can conclude that, if strain and strain relaxation appear as the driving forces for the formation of 3D islands, experiments show that the detailed morphology (*i.e.* size, shape and density of the islands) is less dependent on the misfit than on others growth parameters [1,26,27]. Our experimental results suggest that other factors as surface diffusion, interface energy, elastic coefficients or enthalpy of formation play an important role. As an example, in agreement with the above considerations, InSb dots grown on GaAs [27] exhibit larger dimensions than GaSb dots grown on the same substrate whereas the lattice mismatch is reduced of 7.2% from InSb to GaSb. One has to keep in mind that the surface diffusion processes are also dependent on the nature of the ad-atoms and it is thus not possible to strictly separate the influences of mismatch

and diffusion in these latter studies. Moreover, the relaxation of RFe$_2$(110) layers is assisted by the formation of dislocations that probably influence the detailed morphology of the layers [1].

6 Conclusion

Because of the extraordinary rich properties of $3d/4f$ RFe$_2$ alloys, the control of the fabrication and morphology of epitaxial films is of fundamental and technological interest. However, only few detailed experiments on the growth and related properties of RFe$_2$ compounds have been performed [12–16,18] and the morphology of the epitaxial layer was poorly discussed [17,28].

In this paper, the growth mode of RFe$_2$(110) single crystal layers is first reported. The large parameter mismatch between the RFe$_2$ compounds and the buffer layer leads to the quick formation fully relaxed islands whereas the first monolayers grow strained on the NbFeφ buffer. These successive stages in the growth process (large matched two-dimensional islands or monolayers and relaxed three-dimensional islands on the top of them) are close to the so-called Stranski-Krastanov growth mode, which is consistent with the *ex situ* measured strains [15].

The morphology of DyFe$_2$(110) layers has been investigated, according to the preparation parameters, that are the substrate temperature and the nominal thickness. The morphology evolves from isolated anisotropic dots to a continuous flat surface. The growth occurs in two stages. First, there is nucleation of islands, whose sizes and shapes depend on the preparation parameters. Secondly, the larger islands grow at the cost of smaller ones and coalescence occurs when the deposit goes on. Finally, the morphology is obviously sensitive to the nature of the epitaxial compound: in the thickness range where samples are constituted of islands, an increasing density of dots and a reduction of the dots dimensions are evidenced, changing from DyFe$_2$ to ErFe$_2$.

Because of the interesting magnetostrictive properties of the Laves phases compounds, the as-grown RFe$_2$(110) dots could be a first step towards preparation of nanotransductors or nanoactuators. As an illustration, the magnetization reversal process has been shown to be strongly correlated to the morphologies [17]: continuous DyFe$_2$(110) layers exhibit an anisotropic behaviour with obvious easy and hard magnetization directions, whereas the magnetisation reversal process is likely to be curling in the case of isolated islands. In a near future, the next step could be a better control of the spatial distribution and sizes. Therefore, the use of preferential nucleation sites, *via* the growth on miscut substrates with surface steps and on relaxed templates with dislocations networks, is probably the new challenge.

References

1. W. Seifert, N. Carlsson, M. Miller, M.E. Pisto, L. Samuelson, L.R. Wallenberg, Prog. Crystal Growth Charact. **33**, 423 (1996).
2. R. Nötzel, Semicond. Sci. Technol. **11**, 1365 (1996).
3. D. Eaglesham, M. Cerullo, Phys. Rev. Lett. **64**, 1943 (1990).
4. F.K. LeGoues, M.C. Reuter, J. Tersoff, M. Hammar, R.M. Tromp, Phys. Rev. Lett. **73**, 300 (1993).
5. A. Ponchet, D. Lacombe, L. Durand, D. Alquier, J.M. Cardonna, Appl. Phys. Lett. **72**, 2984 (1998); A. Ponchet, A. Le Corre, H. L'Haridon, B. Lambert, S. Salaun, Appl. Phys. Lett. **67**, 1850 (1995).
6. J.M. Wen, J.W. Ewans, M.C. Bartelt, J.W. Burnett, P.A. Thiel, Phys. Rev. Lett. **76**, 652 (1996).
7. L. Ressier, J.P. Peyrade, C. Vien, J. Appl. Phys. **81**, 2596 (1997).
8. M. Demand, M. Hehn, K. Ounadjela, J.V. Kim, A. Vagov, R.L. Stamps, J. Appl. Phys. **85**, 5498 (1999).
9. C.T. Campbell, Surf. Sci. Rep. **27**, 1 (1997).
10. S. Padovani, F. Scheurer, J.P. Bucher, Europhys. Lett. **45**, 327 (1999); D. Sander, R. Skomski, C. Schmidthals, A. Enders, J. Kirschner, Phys. Rev. Lett. **77**, 2566 (1996).
11. A.E. Clark, in *Magnetostrictive RFe$_2$ compounds*, Vol. 2 of *Handbook on the Physics and Chemistry of Rare Earths*, edited by K. Gschneider, L. Eyring (North Holland, Amsterdam, 1979), Chap. 15.
12. C.T. Wang, R.M. Osgood, R.L. White, B.M. Clemens, in *Magnetic Ultrathin Films, Multilayers and Surfaces*, edited by A. Fert *et al.*, *MRS Symposia Proceedings*, Vol. 384 (Pittsurgh, 1995), p. 79.
13. S. Jaren, E. du Tremolet de Lacheisserie, D. Givord, C. Meyer, J. Magn. Magn. Mater. **165**, 172 (1997).
14. V. Oderno, C. Dufour, K. Dumesnil, Ph. Mangin, G. Marchal, J. Cryst. Growth **165**, 175 (1996).
15. A. Mougin, C. Dufour, K. Dumesnil, N. Maloufi, Ph. Mangin, G. Patrat, Phys. Rev. B **59**, 5950 (1999).
16. A. Mougin, C. Dufour, K. Dumesnil, Ph. Mangin, Phys. Rev. B **62**, 9517 (2000).
17. A. Mougin, C. Dufour, K. Dumesnil, N. Maloufi, Ph. Mangin, Appl. Phys. Lett. **76**, 1449 (2000).
18. M. Hutch, C.P. Flynn, Phys. Rev. B **58**, 11526 (1998).
19. J. Kwo, M. Hong, S. Nakahara, Appl. Phys. Lett. **49**, 319 (1986).
20. I.N. Stranski, L. Krastanov, Sitzungber. Wien. Akad. Wiss. Math-Nat. Kl. IIb **146**, 797 (1938).
21. H. Saito, K. Nishi, S. Sugou, Appl. Phys. Lett. **74**, 1224 (1999).
22. H. Lee, R. Lowe-Webb, W. Wang, P.Cp. Sercel, Appl. Phys. Lett. **72**, 812 (1998).
23. J.A. Venables, Phys. Rev. B **36**, 4153 (1987).
24. J. Tersoff, R.M. Tromp, Phys. Rev. Lett. **70**, 2782 (1993).
25. S. Christiansen, M. Albrecht, H.P. Strunk, H.E. Maier, Appl. Phys. Lett. **64**, 3617 (1994); S. Christiansen, M. Albrecht, H.P. Strunk, P.O. Hansson, E. Bauser, Appl. Phys. Lett. **66**, 574 (1995).
26. D. Leonard, M. Krishnamurthy, S. Fafard, J.L. Merz, P.M. Petroof, J. Vac. Sc. Technol. B **12**, 1063 (1994).
27. B.R. Bennet, R. Magno, B.V. Shanabrook, Appl. Phys. Lett. **68**, 505 (1996).
28. M. Getzlaff, R. Pascal, H. Tödter, M. Bode, R. Wiesendanger, Appl. Surf. Science **142**, 543 (1999).